11712–11726 *Nucleic Acids Research, 2022, Vol. 50, No. 20* *Published online 18 November 2022*
https://doi.org/10.1093/nar/gkac1053

The initiation factor 3 (IF3) residues interacting with initiator tRNA elbow modulate the fidelity of translation initiation and growth fitness in *Escherichia coli*

Jitendra Singh [1,†], Rishi Kumar Mishra[2,†], Shreya Ahana Ayyub [1], Tanweer Hussain [2,*] and Umesh Varshney [1,3,*]

[1]Department of Microbiology and Cell Biology, Indian Institute of Science, Bangalore 560012, India, [2]Department of Molecular Reproduction, Development and Genetics, Indian Institute of Science, Bangalore 560012, India and [3]Jawaharlal Nehru Centre for Advanced Scientific Research, Bangalore 560064, India

Received August 09, 2022; Revised October 18, 2022; Editorial Decision October 20, 2022; Accepted October 24, 2022

ABSTRACT

Initiation factor 3 (IF3) regulates the fidelity of bacterial translation initiation by debarring the use of non-canonical start codons or non-initiator tRNAs and prevents premature docking of the 50S ribosomal subunit to the 30S pre-initiation complex (PIC). The C-terminal domain (CTD) of IF3 can carry out most of the known functions of IF3 and sustain *Escherichia coli* growth. However, the roles of the N-terminal domain (NTD) have remained unclear. We hypothesized that the interaction between NTD and initiator tRNA^{fMet} (i-tRNA) is essential to coordinate the movement of the two domains during the initiation pathway to ensure fidelity of the process. Here, using atomistic molecular dynamics (MD) simulation, we show that R25A/Q33A/R66A mutations do not impact NTD structure but disrupt its interaction with i-tRNA. These NTD residues modulate the fidelity of translation initiation and are crucial for bacterial growth. Our observations also implicate the role of these interactions in the subunit dissociation activity of CTD of IF3. Overall, the study shows that the interactions between NTD of IF3 and i-tRNA are crucial for coupling the movements of NTD and CTD of IF3 during the initiation pathway and in imparting growth fitness to *E. coli*.

INTRODUCTION

Translation initiation from an mRNA bound to the ribosome is a major regulatory step that uses a special tRNA, the initiator tRNA (i-tRNA or fMet-tRNA^{fMet}) and the initiation factors (IF) 1, 2 and 3. The unique features in i-tRNA allow it to participate in initiation (1). The presence of the highly conserved three consecutive GC (3GC) base pairs in its anticodon stem facilitates preferential binding of the i-tRNA into the ribosomal P-site (2). In the classical initiation pathway, bacteria employ three initiation factors, IF1, IF2 and IF3, to assemble the 30S initiation complex (30S IC). IF1 binds at the A-site of 30S and prevents the binding of aminoacyl tRNAs to this site during initiation (3). Further, IF1 enhances the activities of IF2 and IF3 (4). IF2 is a GTPase that helps recruit the i-tRNA to the 30S subunit and promotes the association of the 50S subunit (5,6). IF3 plays a crucial role in the fidelity of translation initiation. It ensures correct recognition of the start codon in mRNA and its pairing with the i-tRNA anticodon in the ribosomal P-site (7,8). Following pairing between the initiation codon and the i-tRNA anticodon, IF3 is displaced from the P-site, allowing docking of the 50S subunit. Subsequently, IF3 is ejected from the assembly to form the 70S complex comprising 30S and 50S ribosomal subunits, mRNA and i-tRNA (9–12).

IF3 consists of an N-terminal domain (NTD) and a C-terminal domain (CTD) linked through a flexible lysine-rich inter-domain helix linker (13,14). The NTD lies on top of the platform of the 30S subunit near the ribosomal protein, uS11. The NTD makes minimal interaction with the 30S, and a significant portion of it lies away from the 30S sub-

*To whom correspondence should be addressed. Tel: +91 80 22932686; Email: varshney@iisc.ac.in
Correspondence may also be addressed to Tanweer Hussain. Tel: +91 80 22933262; Email: hussain@iisc.ac.in
†The authors wish it to be known that, in their opinion, the first two authors should be regarded as Joint First Authors.
Present address: Shreya Ahana Ayyub, Department of Physical Biochemistry, Max Planck Institute for Multidisciplinary Sciences, Am Fassberg 11, 37077 Göttingen, Germany.

unit. The linker helix spans the region from the platform to the P site and interacts with h23 and h24. The CTD is located near the h44, closer to the P-site. It interacts with h44, h24 and h45 (12,15), and clashes with this position's binding site for H69 of the 50S subunit. Thus, the CTD is responsible for the anti-association activity of IF3 (16). It is proposed that IF3 indirectly modulates the A-minor interactions of G1338 and A1339 of 16S rRNA with the 3GC base pairs in i-tRNA (17), and IF3 is known to prevent initiation with tRNAs lacking the 3GC base pairs (18).

IF3 prevents pseudo-initiation complex formation and initiation from non-canonical start codons (19,20). Mutations in IF3 allow initiation from non-canonical codons (18,21–23). It was proposed that the CTD performs all the functions of IF3, and the NTD merely provides the thermodynamic stability to the molecule (19). Recently, we showed that although the CTD is necessary and sufficient to sustain *E. coli* cells for growth, the NTD plays a crucial role in the fidelity of initiation (24). Several mutants of Y75 residue present in the NTD/linker were also found to be compromised in the fidelity of initiation (21). However, the mechanism of how the NTD plays a role in the fidelity of initiation remains unknown.

Recent cryo-EM studies show that the NTD makes contacts with the elbow region of i-tRNA in 30S PICs (12,15) and follows the movement of i-tRNA during its accommodation in the P-site (12,15). However, the *in vivo* relevance of the interaction between the NTD and the elbow region of i-tRNA has remained unclear. To further our understanding of the role of the NTD in initiation, especially in the context of i-tRNA–IF3 interactions, we carried out site-directed mutagenesis of the key residues in the NTD. We show through MD simulations that the mutations in conserved residues of NTD disrupt its interaction with i-tRNA. Further, we found that disrupting these interactions affects the fidelity of translation initiation and i-tRNA recognition. And the CTD displacement from the P-site is crucial for 50S recruitment. The studies reveal a crosstalk between the NTD and CTD to maintain growth fitness of *E. coli*.

MATERIALS AND METHODS

Structural analysis and molecular dynamics (MD) simulations

As the structure of full length *E. coli* IF3 (*Eco*IF3) is not available, we performed homology modelling of *Eco*IF3 using *Thermus thermophilus* IF3 structure in 30S IC (PDB ID: 5LMN) as a template in Robetta online server. The model obtained from Robetta was used for simulation of full-length IF3. For simulation of the N-terminal domain of IF3 (NTD), we used residues R11 to Y70 (*E. coli* numbering). The system for simulation of the i-tRNA–NTD complex was prepared by superposing homology modelled NTD and i-tRNA structure (PDB ID: 6O7K) on IF3 and i-tRNA present in the structure of *T. thermophilus* 30S pre-IC (PDB ID- 5LMQ) (12,25). For simulation of the mutants, i.e. NTD (R25A,Q33A and R66A) and i-tRNA-NTD (R25A, Q33A and R66A), mutations were created in Pymol. The modifications on i-tRNA (T54, Ψ55) were omitted for the simulation studies as T54 does not interact with NTD and the interaction of NTD residues (R25 and Q33) with Ψ55 is only through the phosphate backbone, and there is no involvement of the modification on the base. Cubic simulation boxes of sides 7 nm (NTD (WT) and NTD (R25A/Q33A/R66A)), 10 nm (IF3) and 8 nm [i-tRNA-NTD (WT) and i-tRNA-NTD (R25A/Q33A/R66A)] were used to simulate TIP3P solvated wild type molecules as well as their mutants. Each system was charge equilibrated with addition of K^+ ion and final salt concentration was maintained at ∼150 mM KCl. Energy minimization was done using the steepest gradient descent algorithm Verlet cut-off scheme. Temperature and pressure equilibrations were applied for 100 ps each using Berendsen Thermostat and Barostat. Amberff14SB (26), and χOL3 (27) force fields were used for proteins, and RNA, respectively. All simulations were assembled and run independently thrice for 1 μs each, and the trajectories were analysed on Pymol using Plumed (28). Average structures were calculated using frames from 500 ns to 1 μs with the frames extracted at every 10 ns interval.

Bacterial strains and plasmids

Bacterial strains and plasmids used are listed in Supplementary Tables S1 and S2, respectively. Cultures were grown in Luria-Bertani (LB) broth or LB-agar plates containing 1.8% Bacto-agar (Difco). Cultures were supplemented with ampicillin (Amp, 100 μg/ml), chloramphenicol (Cm, 30 μg/ml), kanamycin (Kan, 25 μg/ml) or tetracycline (Tet, 7.5 μg/ml) as required.

Generation of NTD mutants

The NTD mutants were generated in pACDH*Eco*IF3 (Kan^R). The site-directed mutagenesis primers were 5' end phosphorylated by polynucleotide kinase and used in PCR with the plasmids as follows: 94°C for 5 min followed by 25 cycles of 94°C for 1 min, 50°C for 30 s, 70°C for 10 min 10 s followed by a final extension at 70°C for 10 min. PCRs were carried out using 10 pmol of each primer and 250 μM dNTPs in 20 μl volumes, followed by over-night treatment with DpnI (NEB) and introduced into *E. coli* TG1 by transformation. The putative clones were verified by DNA sequencing.

Genetic manipulation of bacterial strains

pACDH (Kan^R) carrying the wild type or mutant IF3 genes were used to amplify the IF3 gene (*infC*) along with the kan^R marker and the amplicon was recombined at the *chb* locus using λ-red recombineering (29). The kan^R cassette linked with the IF3 gene (at *chb* locus) was then changed with a tet^R cassette using the same λ-red recombinase strategy. Deletion of the wild type *infC* was performed using P1 phage lysate generated on KL16 Δ*infC fs*::kan^R/pACDHEcoIF3 strain (24). All constructs were confirmed by PCR and DNA sequencing.

Growth curve analysis

Four replicates of each strain were grown till saturation at the specified temperatures and desired antibiotics. A

thousand-fold diluted cultures (200 μl) were transferred to honeycomb plates and placed in automated Bioscreen C growth reader, which measured OD_{600} every hour. Mean OD values and the standard deviations were calculated, and the data were plotted with Time on X-axis against OD_{600} on Y-axis using GraphPad Prism.

Northern blotting

Total RNA was separated on 2.2% agarose gel using 1X TBE (89 mM Tris, 89 mM boric acid, 2 mM Na_2EDTA) at 80 V for 2 h. RNA was transferred to Hybond-XL (Amersham) membrane using semi-dry trans-blot apparatus (Bio-Rad) at 5 V for 3 h. The blot was kept for blocking in 1× prehybridization buffer [2× prehybridization buffer contains 10× Denhardt reagent [0.2% Ficoll 400 (w/v), 0.2% polyvinylpyrrolidone (w/v), 0.2% bovine serum albumin], 10× SSC (1.5 M NaCl, 0.3 M sodium citrate), 30 mg/100 ml yeast RNA, 1% SDS] at 65°C. The ^{32}P-5' end labelled probe was added and kept overnight at 43°C. The blot was then washed in three consecutive steps with buffer I (4× SSC, 0.1% SDS); buffer II (2× SSC, 0.1% SDS); and buffer III (1× SSC) for 30 min each at 43°C, exposed to phosphor-imager screen and analyzed on BioImage Analyzer (FLA5100, Fuji Film).

Chloramphenicol acetyltransferase (CAT) assay

The CAT assays were performed as before (30). Briefly, 11 μl of diluted or undiluted lysate was mixed with 15.5 μl of reaction mix (500 mM Tris–HCl, pH-8.0, 5 nmol chloramphenicol, 0.05 μCi ^{14}C-chloramphenicol (Sp. activity 57.8 mCi mmol; ARC) and the reaction was started with addition of 3.5 μl of acetyl CoA (3.5 mg/ml). After 20 min of incubation at 37°C, the reaction was stopped using 300 μl ethyl acetate. After centrifugation, 200 μl of the supernatant was vacuum dried and spotted on a silica gel 60 plate (Merck). Thin layer chromatography (TLC) was performed using mobile phase consisting of chloroform and methanol in a 95:5 (v/v) ratio. The TLC plate was scanned post 6 h exposure using a Bio-Image Analyzer (FLA5000, Fujifilm). The densitometric analysis for quantification was done using Multi Gauge V2.3.

Western blotting

The total proteins separated on 12.5% SDS-PAGE were transferred onto methanol wetted polyvinylidene difluoride (PVDF) membrane (Amersham) using transfer buffer (25 mM Tris, 192 mM glycine, 0.1% SDS, pH 8.3 with 15% methanol). The membrane was blocked with 5% skimmed milk in 1× TBST (20 mM Tris–HCl, pH 7.5, 0.9% NaCl and 0.2% v/v Tween 20) under rocking at room temperature for 2 h, incubated with IF3 antibodies (1:5000) overnight at 4°C and washed thrice with TBST and incubated with the secondary antibody (1:5000 α-rabbit IgG-HRP, Genei) in 1× TBST for 2 h. Again, the blot was washed thrice with 1× TBST, developed using ECL reagent (Millipore) and scanned in Chemi Doc (GE).

Polysome profiling

E. coli cultures at OD_{600} of 0.6 were treated with Cm (140 μg/ml) and incubated for 10 min. Cultures were chilled in the salt-ice mix and the cells were pelleted at 8000 rpm for 10 min. The cell pellet was washed once with 1 ml buffer A (20 mM Tris–HCl, pH 8.0, 100 mM NH_4Cl, 7 or 10 mM $MgCl_2$, 3 mM DTT, 10% sucrose) and resuspended in 1 ml buffer A. The cells were lysed by addition of lysozyme to a final concentration of 0.75 μg/ml and incubated on ice for 1 h. The samples were flash frozen in liquid nitrogen and thawed in cold room twice and stored in –80°C overnight. The samples were thawed in cold room and centrifuged at 13 000 rpm for 30 min to remove cell debris. The supernatant was stored in 1 ml aliquots at –80°C after flash freezing in liquid nitrogen. Polysome lysate corresponding to 20 OD_{260} was layered on top of 15–35% continuous sucrose gradient, prepared using BioComp gradient maker. The samples were centrifuged at 36 000 rpm for 5 h using a SW41Ti rotor. After the run, the gradient was analyzed using BioComp Gradient Analyzer and simultaneously the fractions (400 μl) were collected using GILSON FC203B fraction collector.

Purification of 30S subunit and initiation factors

The whole process of 30S ribosomal subunit purification from *E. coli* MG1655 was performed at 4°C. Cell pellet at mid log phase was resuspended in cell opening buffer (20 mM Tris, pH-7.6, 100 mM NH_4Cl, 10 mM $MgCl_2$ and 3 mM β-mercaptoethanol) and lysed by sonication. Crude ribosomes were isolated by loading S-30 lysate on 1.1 M sucrose cushion twice. Total ribosomes were then incubated in ribo-dissociation buffer (20 mM Tris, pH 7.6, 60 mM NH_4Cl, 1.5 mM $MgCl_2$, 3 mM β-mercaptoethanol, 2 mM puromycin) and loaded on 10%-30% sucrose density gradient. 30S fractions were collected, pelleted, and resuspended in ribo-storage buffer (50 mM Tris, pH-7.6, 70 mM NH_4Cl, 7 mM $MgCl_2$, 30 mM KCl). His tagged versions of IF1, IF2, IF3 (WT) and IF3 (R25A/ Q33A/ R66A) were purified by standard Ni-NTA affinity purification followed by gel filtration.

IF3-30S binding assay

The 30S ribosomes were activated by incubating them at 37°C for 30 min. One μM 30S, 1 μM IF1, 2.5 μM IF2 and 2.5 μM of either IF3 (WT) or IF3 (R25A/Q33A/R66A) were mixed and incubated at 37°C for 30 min. The mixture was loaded on 10–30% sucrose density gradient to isolate IF3 bound 30S fractions. The bound IF3 levels were then checked by western blot using anti-his antibodies.

RESULTS

Design of the mutations in the NTD of IF3 and their effects on structure

The analysis of the cryo-EM structures (PDB ID – 5LMQ, 5LMR, 5LMS, 5LMT, 5LMU and 5LMV) of initiation complexes (12) revealed that the NTD residues R25 (Arg25), Q33 (Gln33) and R66 (Arg33) (*E. coli* numbering) interact transiently with the i-tRNA bases G19, Ψ55,

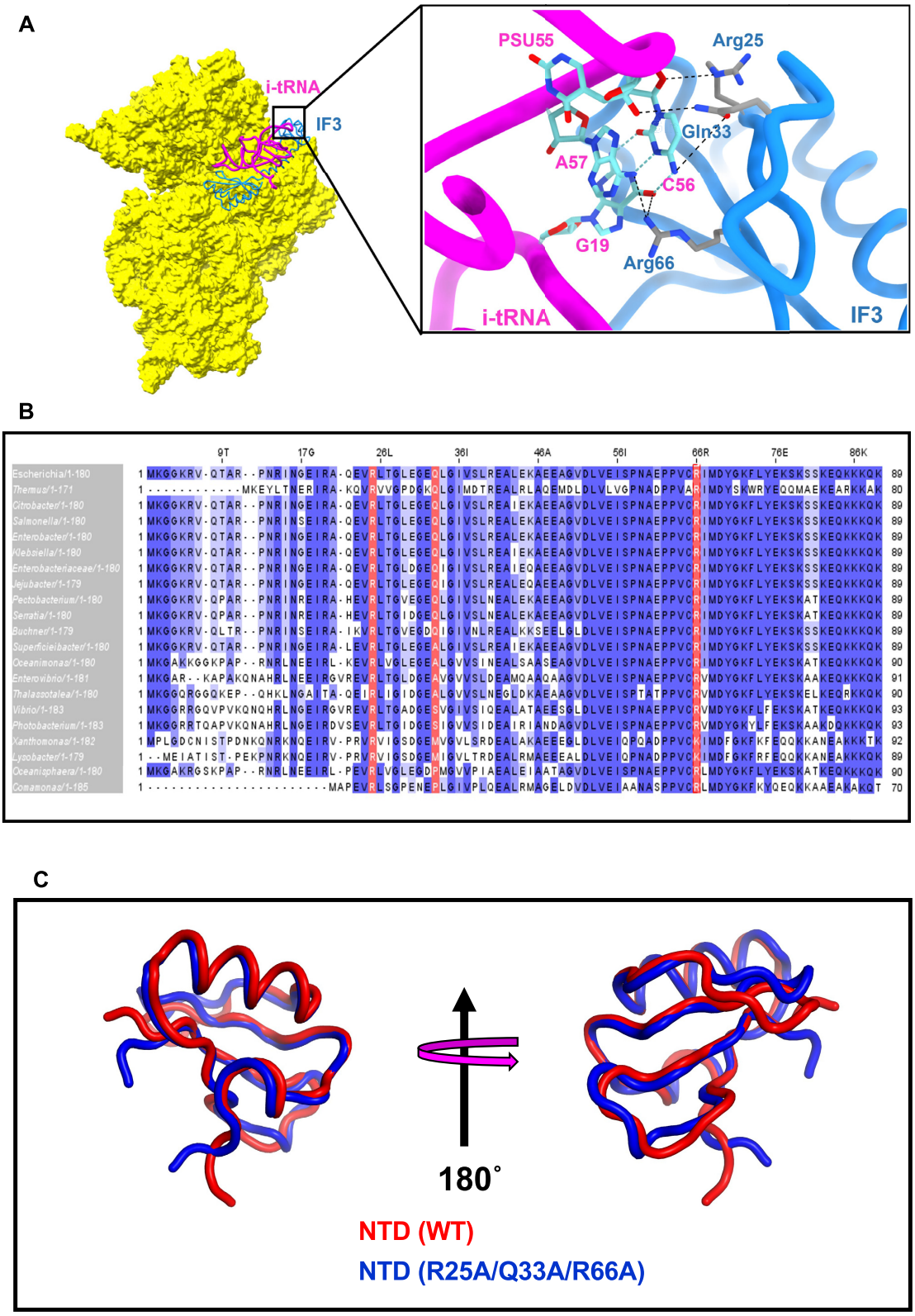

Figure 1. Interactions of IF3 with i-tRNA. (**A**) Interaction of R25, Q33 and R66 (*E. coli* numbering) of IF3 with the corresponding nucleotides in i-tRNA (adapted from PDB 5LMQ). (**B**) Multiple sequence alignment of IF3 from different bacterial species shows R25 to be invariant while R66 is well conserved. However, Q33 is replaced by A/S/M/P in many bacteria (red). (**C**) Comparison of average structures of NTD (WT) (Red) and NTD (R25A/Q33A/R66A) (Blue) shows no change in the overall average structure of NTD due to the mutations (RMSD of alignment 1.2 Å).

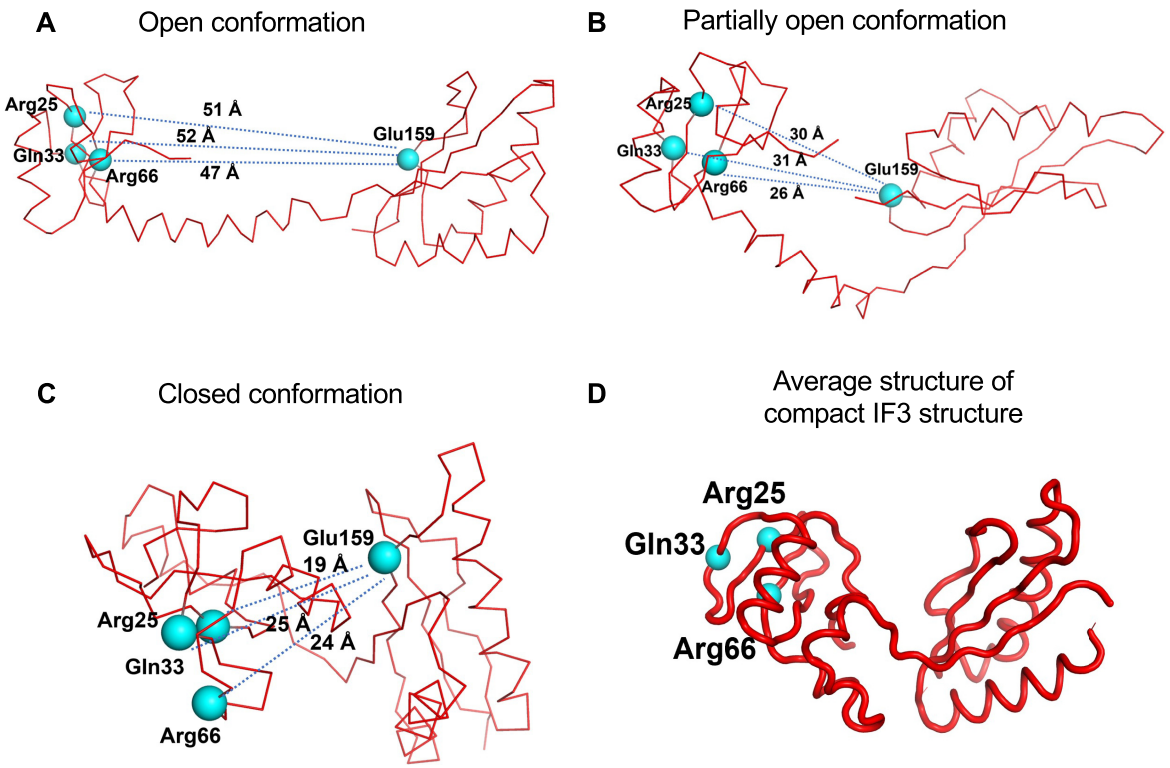

Figure 2. Simulation of full-length IF3. Representative snapshots of IF3 showing (**A**) open conformation, (**B**) partially open conformation and (**C**) closed conformation. (**D**) Representation of residues R25, Q33 and R66 as spheres in the average structure of the closed conformation of IF3 showing the location of these residues facing the solvent and away from the interdomain interface of IF3.

C56 and A57 (Figure 1A; PDB ID: 5LMQ; and Supplementary Table S3) during different stages of i-tRNA accommodation into the P-site. Notably, in contrast to R25 and R66 which show interaction with the i-tRNA bases in all the stages of i-tRNA accommodation, Q33 interacts with it only during some stages (Supplementary Table S3). Further, the residue R25 is invariant, and R66 is well conserved in different bacterial IF3 proteins analysed, while Q33 is occasionally replaced with amino acids like Ala, Met, Pro and Ser (Figure 1B). To evaluate any structural changes in the NTD due to the mutations at R25, Q33 and R66, we performed atomistic MD simulations of the NTD (WT) and NTD (R25A/Q33A/R66A) (Supplementary Figures S1A). The average structures show no significant difference between NTD (WT) and NTD (R25A/Q33A/R66A) (Figures 1C; Supplementary Figures S1B).

Effect of the NTD mutations on the interactions between NTD and CTD

To study the interaction between the two domains of IF3, we performed the simulation runs of 1 μs, where we started with the structure of IF3 in a stretched conformation like the conformation in PDB-5LMN (Figure 2). As reported previously, by FRET studies and MD simulations (31–33), we observed three different conformations of IF3 in simulation runs: open (where NTD and CTD are far apart), partially open (NTD and CTD are relatively closer) and closed (NTD and CTD are at the closest distance) (Figures 2A–C). We then looked at the distances of the residues R25, Q33 and R66 with the CTD residues of IF3 in all conformations. Although the transient interactions between the two domains in the closed state cannot be ruled out, the residues (R25, Q33 and R66) occupy the solvent side of free IF3 in all the conformations and are far from the interface of NTD and CTD (Figure 2A–D). Therefore, these residues do not contribute to interactions between NTD and CTD. Thus, the mutations in these residues are unlikely to impact the interdomain interactions. These results agree with the NMR spectroscopy performed on IF3 in solution (13). The two domains of IF3 are structurally independent and separated by a flexible linker. As the NTD mutations do not affect the overall structure of NTD (Figure 1C) and face away from the interdomain interface (Figure 2D), they are unlikely to have an impact on the interaction between the NTD and CTD.

Effect of NTD mutations on i-tRNA-NTD interaction

For studying the effect of R25A, Q33A and R66A mutations on the interaction between NTD and i-tRNA, we performed MD simulations of i-tRNA-NTD (WT) and i-tRNA-NTD (R25A/Q33A/R66A) complex (Figure 3 and Supplementary Figure S2A). We observed that the interaction between NTD (WT) residues and i-tRNA remains stable during the simulation (Figures 3A-3D, left panels)

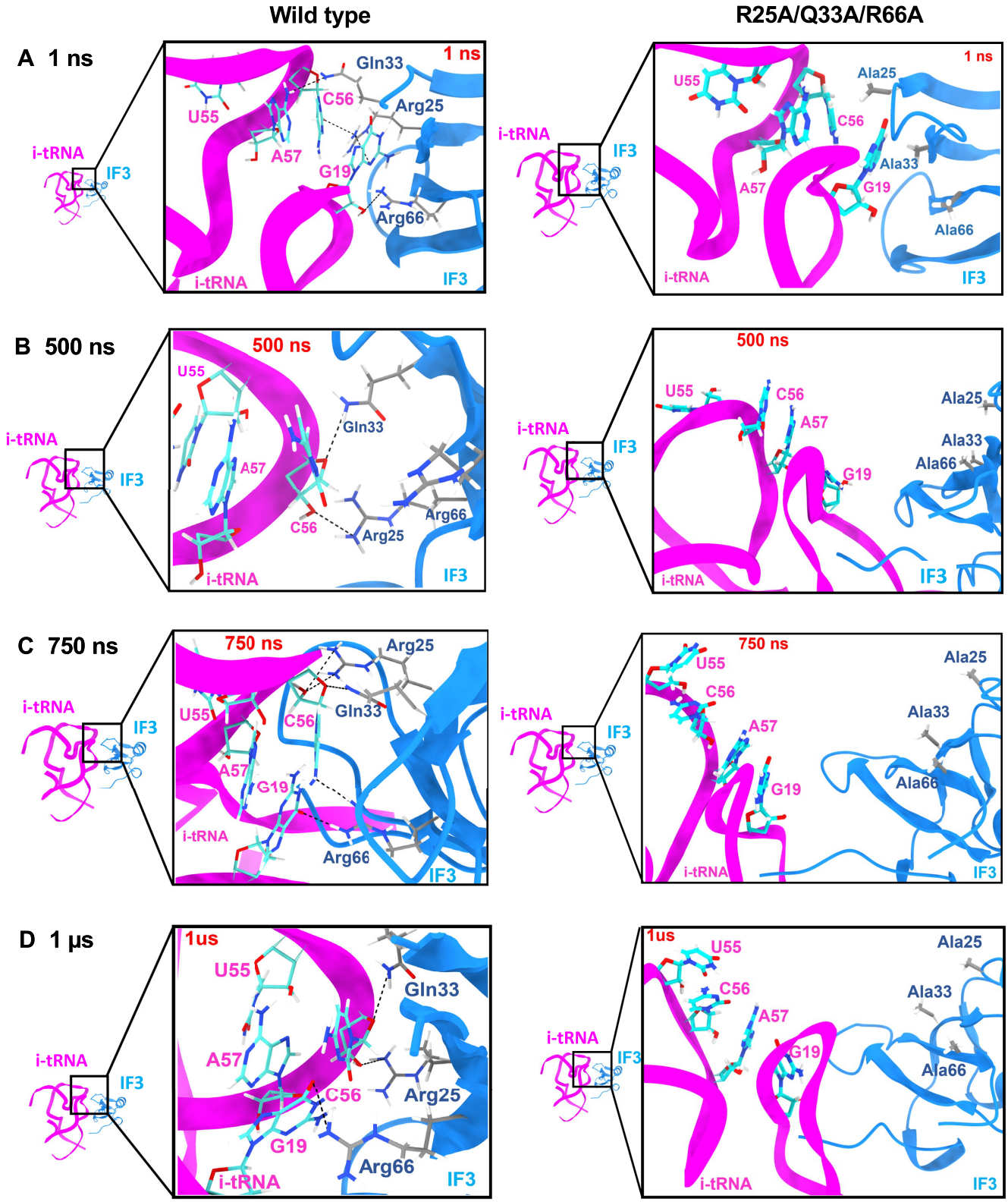

Figure 3. Comparison of the distance between the interacting residues of NTD and i-tRNA between NTD (WT) (left panels) and NTD (R25A/Q33A/R66A) (right panels) during the simulation after 1 ns (**A**), 500 ns (**B**), 750 ns (**C**) and 1 μs (**D**).

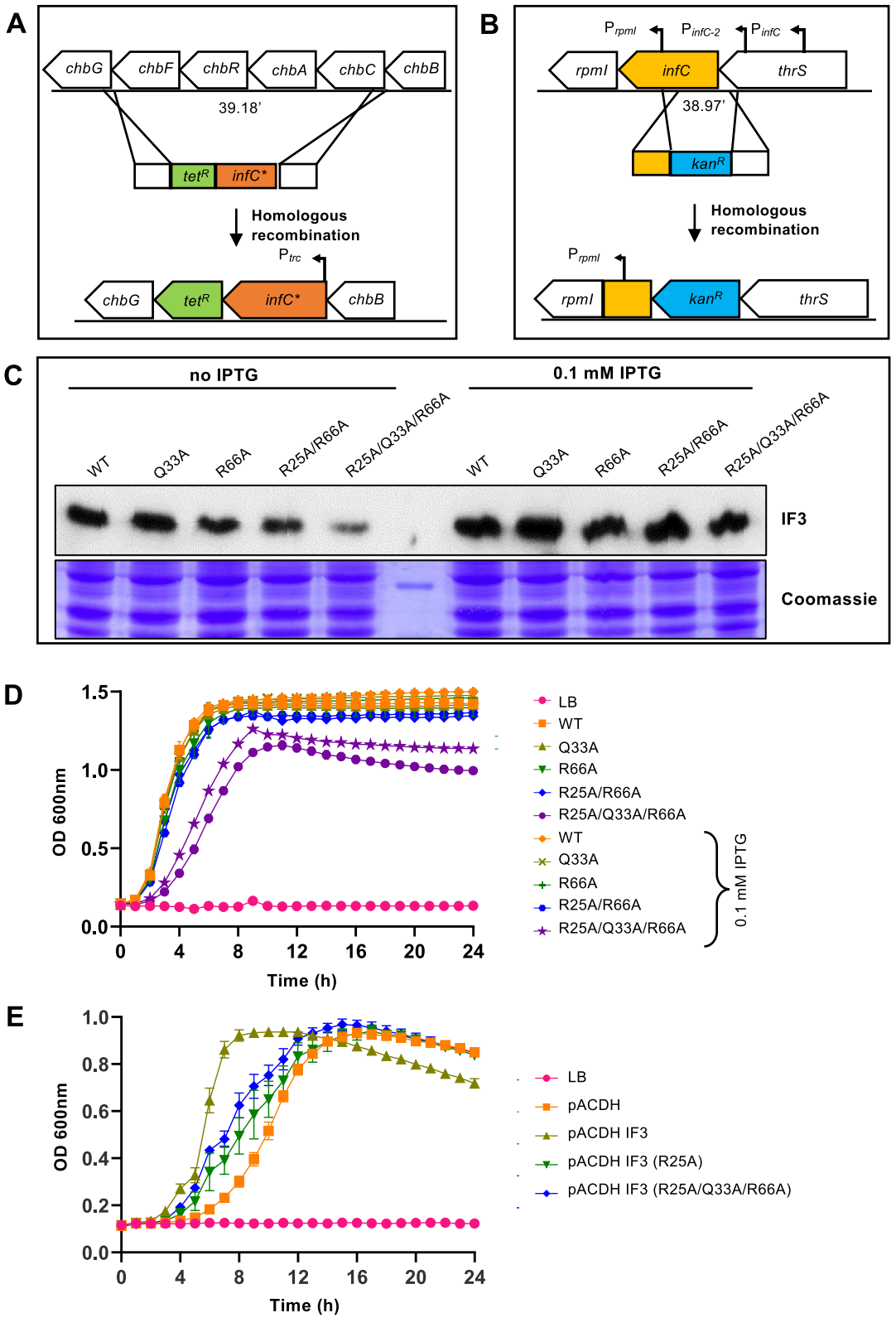

Figure 4. Generation of *E. coli* strains harbouring the IF3 mutant alleles and their growth. (**A**) Diagrammatic representation of the *chb* locus and insertion of *infC tet*^{R} cassette in this position. (**B**) Partial deletion of *infC* locus using KL16 *infC fs*:: *kan* (Supplementary Table S1). (**C**) Western blot for IF3 in different IF3 strains without or with IPTG induction. (**D**) Growth of the strains sustained on the *infC* alleles at the *chb* locus without or with IPTG induction at 37°C. (**E**) Growth of the KL16 *infC* Δ55:: *kan* strains harbouring plasmid borne copies of IF3 genes (WT), IF3 (R25A) and IF3 (R25A/Q33A/R66A) at 37°C.

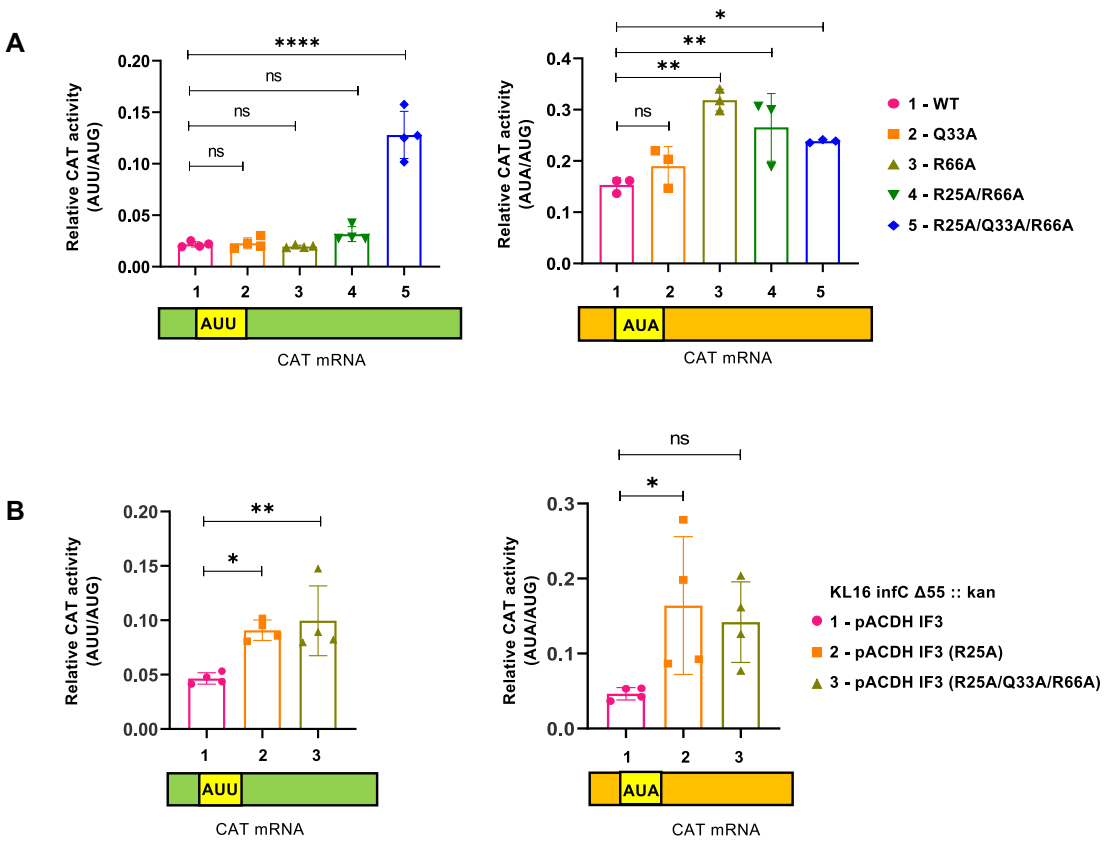

Figure 5. Initiation assays for the non-canonical start codons. (**A**) CAT assays for AUU start codon (*left panel*) and AUA start codon (*right panel*) for different IF3 mutants expressed from the *chb* locus. (**B**) CAT assays for AUU start codon (*left panel*) and AUA start codon (*right panel*) for different plasmid borne copies of the IF3 mutants in KL16 *infC* Δ55:: *kan*. Bars represent mean ± SD for $n = 4$. *P* values, $^{*}P < 0.05$; $^{**}P < 0.01$; $^{***}P < 0.001$; $^{****}P < 0.0001$ indicate significant differences between samples; 'ns' represent not significant.

while in the case of NTD (R25A/Q33A/R66A), the interactions are disrupted, and the NTD (R25A/Q33A/R66A) move away from i-tRNA residues (G19, U55, C56, A57) (Figures 3A–D, right panels). These observations were further strengthened by the calculation of the distance between the Centre of Mass of NTD residues (R25/A25, Q33/A33 and R66/A66) and the interacting i-tRNA residues (G19, U55, C56, A57) over the course of simulations (Supplementary Figure S2B). Analysis of the mean of distance between Cα of NTD residues (R25, Q33 and R66) and all individual atoms of G19, U55, C56 and A58 nucleotides of i-tRNA present at the interface over the simulation of 1 μs shows a higher distance in case of mutant compared to the wild type, which indicates loss of interaction between i-tRNA and NTD (R25A/Q33A and R66A) (Supplementary Figures S2C-S2E). Analysis of the dynamics of hydrogen bonds at the interface of NTD and i-tRNA during simulation suggests that the i-tRNA–NTD (WT) complex has extensive hydrogen bonding at the interface, but for the i-tRNA-NTD (R25A/Q33A/R66A), there is a decrease in the number of hydrogen bonds (Supplementary Figures S3A–C). These observations indicate a compromise in the stability of the complex with the NTD (R25A/Q33A/R66A). Further analysis of the dynamics of the bridges between nitrogenous bases and phosphates within i-tRNA during simulations shows that the WT and the mutant complexes share most base-phosphate bridges (Supplementary Table S4). Also, we noted that almost all residue pairs making sugar-phosphate interactions within i-tRNA in both WT and mutants are common, except that a few of the pairs are exclusive to either WT or the mutant (Supplementary Table S5). Since there are only minor differences in the intramolecular interactions in i-tRNA, the overall structure of i-tRNA does not change during the simulations. Thus, simulation studies of the complexes of i-tRNA with the NTD (WT) and the NTD (R25A/Q33A/R66A) suggest that the mutations in NTD disrupt its interactions with i-tRNA. As the mutant NTD loses contact with i-tRNA, it is unlikely to move in concert with i-tRNA during the initiation pathway, unlike as observed earlier (12,15). Hence, we hypothesize that these mutations may lead to a loss of coordination between the IF3 NTD and CTD movements and affect the fidelity of translation initiation.

Generation and growth analysis of the strains harbouring IF3 NTD mutants

Based on the computational analyses (Figures 1–3), to investigate the role of IF3 NTD by specifically disrupting IF3 interaction with the i-tRNA elbow, we mutated R25, Q33

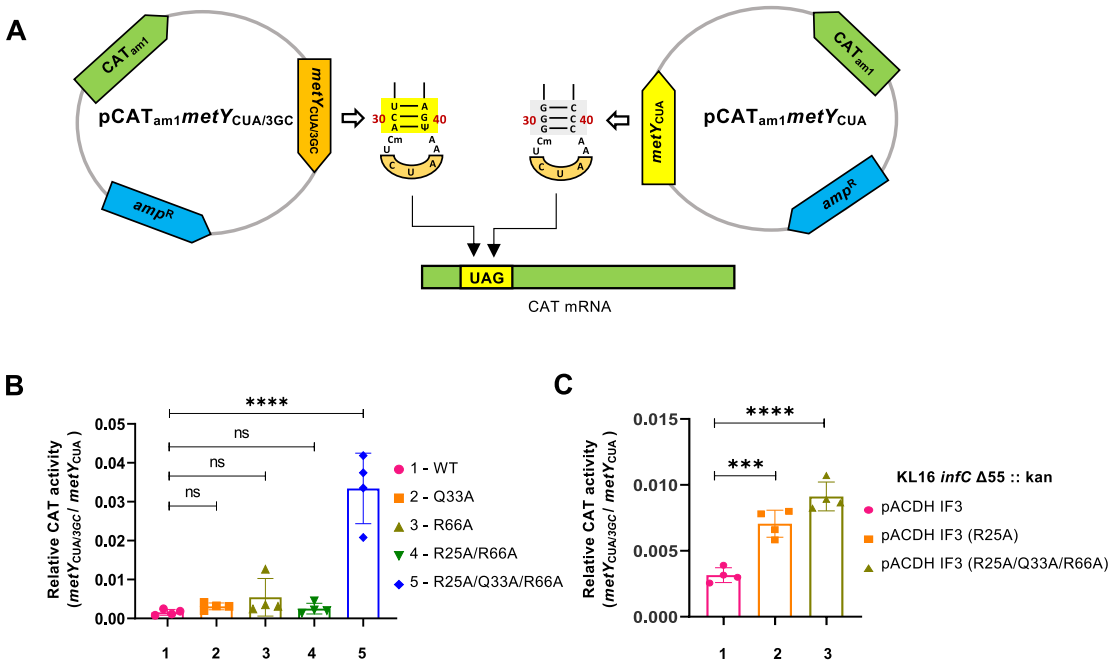

Figure 6. Initiation with the 3GC mutant i-tRNA. (**A**) Schematic of initiation with 3GC mutant i-tRNA from the CAT reporter. (**B**) Initiation with the 3GC mutant i-tRNA in the strains with mutant alleles of *infC* at the *chb* locus. (**C**) Initiation with the 3GC mutant i-tRNA in KL16 *infC* Δ55:: *kan* strains harbouring the mutant IF3 genes on plasmid. Bars represent mean ± SD for $n = 4$. *P* values, $^{*}P < 0.05$; $^{**}P < 0.01$; $^{***}P < 0.001$; $^{****}P < 0.0001$ indicate significant differences between samples; 'ns' represent not significant.

and R66 to Ala (R25A, Q33A and R66A) mutations. A double (R25A/R66A) and a triple (R25A/Q33A/R66A) mutants were also made. We then generated *E. coli* mutants harbouring IF3 gene (*infC*) alleles linked with a tet^R marker at the non-essential *chb* locus in (Figure 4A). Subsequently, the *infC* gene from its original locus in the chromosome was disrupted with a kan^R marker (Figure 4B). As shown in the figure, the *rpmI* promoter lies within the *infC* ORF (34). Thus, to avoid any polar effects on the expression of the downstream genes while disrupting the native *infC*, we employed the approach established in our earlier study (24) of P1-phage mediated transductions to replace the *infC* with *infC*fs::*kan* wherein the first 55 amino acids of IF3 are replaced by the kan^R cassette such that the downstream region is not in frame with the sequences of the inserted cassette (Figure 4B). The final strains sustain solely on the chromosomally located IF3 gene at the *chb* locus (Supplementary Table S1). However, for unknown reasons, despite using multiple approaches, we were unable to generate a strain sustained on IF3 (R25A) alone. Nonetheless, the R25A mutation could be introduced in the genome in combination with the other mutations (Q33A, R66A) to sustain the growth of the strains. In addition, we were able to investigate the impact of the R25A mutation in a strain sustained on the CTD of IF3.

To characterize the strains, we investigated the levels of IF3 (wild type or mutants) expression in them (Figure 4C) and their growth (Figure 4D). Except for a lower level of expression of the IF3 (R25A/Q33A/R66A) mutant, we observed a similar level of expression of the other mutants (Q33A, R66A and R25A/R66A) when compared with the wild type IF3 (Figure 4C, no IPTG). However, upon induction with IPTG, the deficiency in the level of expression of the (R25A/Q33A/R66A) mutant could be rescued (Figure 4C, 0.1 mM IPTG). Next, we checked the growth of the strains sustained on the IF3 mutants (expressed from the *chb* locus). We found that the strain sustained on the (R25A/Q33A/R66A) mutant was compromised for its growth (Figure 4D), although induction with IPTG resulted in its partial rescue (Figure 4D).

As we were unable to sustain the strain on R25A mutant from the *chb* locus, we used the *infC*Δ55 (also referred to as Δ55) strain, which is sustained on the CTD of IF3 and grows slowly, allowing us to study functions of the plasmid encoded IF3 genes. We earlier showed that the growth defect of the Δ55 strain is completely rescued upon the expression of a plasmid-borne wild type IF3 (24). Even in this background, the IF3 (R25A) and IF3 (R25A/Q33A/R66A) mutants were unable to rescue the growth defects of the Δ55 strain to the wild type IF3 level (Figure 4E). Overall, the data show that mutating R25 alone or together with Q33 and R66 compromises the function of IF3 and suggest that R25, which is highly conserved across bacterial species (Figure 1B), plays an important role in IF3 function.

NTD of IF3 regulates start codon selection

Selection of a correct start codon by i-tRNA, a determining step in establishing the reading frame in an mRNA, is crucial for translation fidelity. The AUG codon is the most common start codon, followed by GUG and UUG codons (35). IF3 promotes initiation from the commonly used start codons and impedes the usage of less commonly used start codons like AUU and AUA (36). Earlier, we reported the

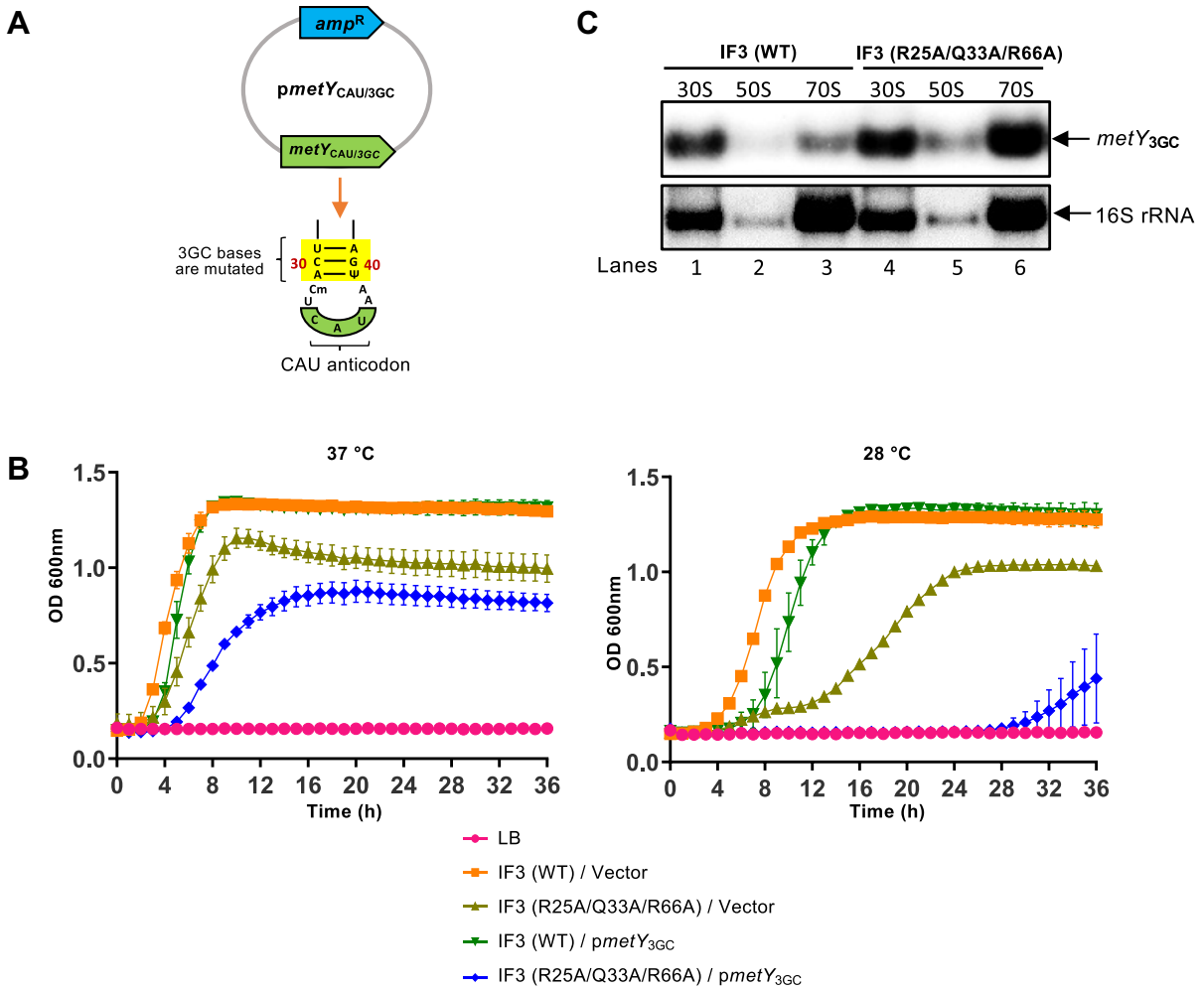

Figure 7. Overexpression of the 3GC mutant i-tRNA having wild type anticodon (CAU). (**A**) Plasmid used to overexpress the 3GC mutant i-tRNA. (**B**) Growth curves of strains harbouring the 3GC mutant i-tRNA plasmid in the strains harbouring various alleles of *infC* (WT or R25A/Q33A/R66A) at *chb* locus, at 37°C (*left*) and 28°C (right). (**C**) Northern blot for the 3GC mutant i-tRNA and 16S rRNA in different ribosomal fractions from the same strains.

involvement of the NTD in initiation codon selection by IF3 (24). To investigate if mutating the amino acids in the NTD that interact with the elbow region of i-tRNA influences the codon selection, we introduced plasmid-borne reporter genes of chloramphenicol acetyltransferase (CAT) having different initiation codons in the strains sustained on the various IF3 mutants and assayed CAT activities as a measure of initiation (24,37). Initiation with the AUU start codon increased about 5-fold in the background of the R25A/Q33A/R66A mutant IF3 (Figure 5A, left panel; compare bars 1 and 5; and Supplementary Table S6). Likewise, initiation with AUA codon increased about 1.5 to 2-fold in the strain backgrounds of R66A, R25A/R66A and R25A/Q33A/R66A mutant IF3 (Figure 5A, right panel; compare bars 3, 4, 5 with bar 1; and Supplementary Table S6). However, the Q33A mutation alone did not show a significant impact (Figure 5A, right panel; bar 2). We then used the Δ55 strain, which showed an increased initiation from the non-canonical start codons, and expression of the wild type IF3 reduced it to the levels observed in the wild type strain (24). However, neither R25A nor R25A/Q33A/R66A mutants restored the fidelity of initiation codon selection in the Δ55 strain (Figure 5B; and Supplementary Table S7). These observations suggest that the interactions between i-tRNA and the NTD play an important role in start codon discrimination, and a perturbation of these interactions results in failure to avoid initiation from the non-canonical start codons.

NTD of IF3 contributes to the scrutiny of the 3GC base pairs in i-tRNA selection

IF3 allows initiation complexes containing i-tRNA and efficiently rejects those with non-initiator tRNAs from the 30S ribosomes. The highly conserved 3GC base pairs in the anticodon stem of i-tRNA are crucial for its IF3-mediated selection over other tRNAs (17,18,24). To investigate how mutations in the NTD may influence this role, we studied initiation using the 3GC mutant i-tRNA in CATam1 reporter assay (Figure 6A) (38). Initiation with the 3GC mutant i-

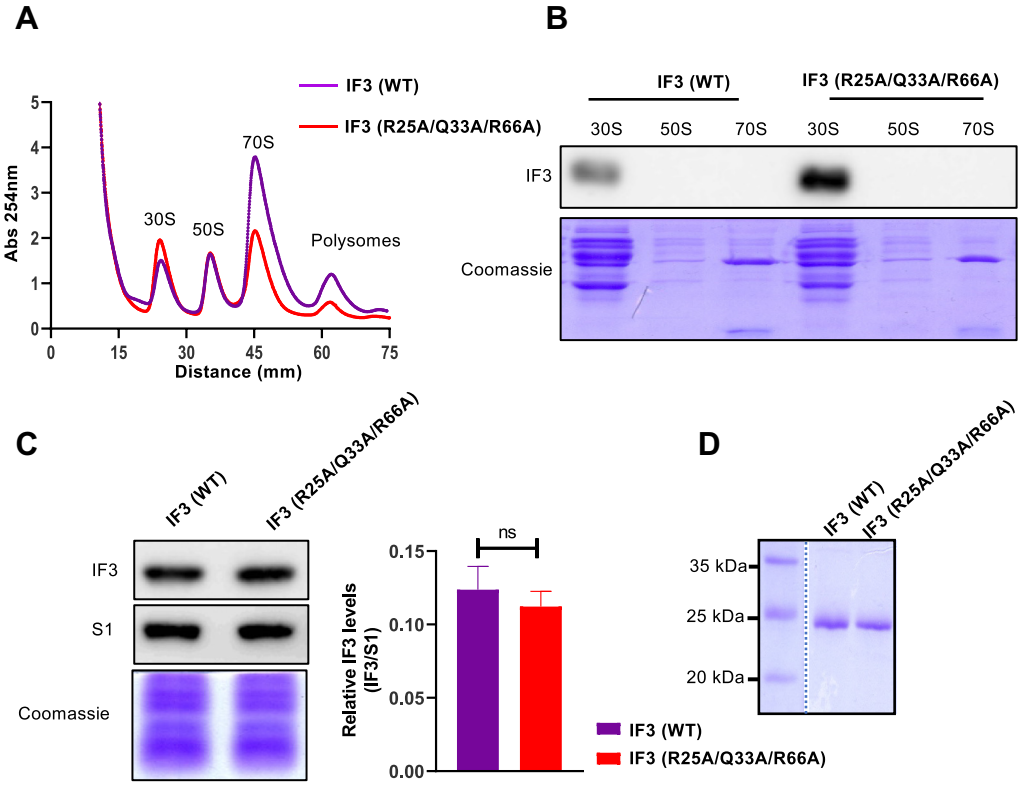

Figure 8. Effect of IF3 NTD mutations on IF3 binding to 30S. (**A**) Polysome profiles separated on a 15–35% sucrose density gradient for strains harbouring IF3 (WT) or IF3 (R25A/Q33A/R66A). (**B**) Western blot analysis for IF3 present in different ribosomal fractions isolated from the polysome profiles in (A). (**C**) *in vitro* binding of IF3 (WT) or IF3 (R25A, Q33A, R66A) with purified 30S in presence of IF1 and IF2. (**D**) SDS-PAGE showing equal amount of IF3 (WT) or IF3 (R25A/Q33A/R66A) used for the *in vitro* assay.

tRNA in the R25A/Q33A/R66A mutant sustained strain was significantly higher than the other strains (Figure 6B; and Supplementary Table S8). Likewise, in the Δ55 strain harbouring the mutant (R25A or R25A/Q33A/R66A) allele of IF3, initiation with the 3GC mutant i-tRNA was higher than those harbouring the wild type allele of IF3 (Figure 6C; and Supplementary Table S7).

In another approach to investigate the role of IF3 in the scrutiny of the 3GC pairs in the anticodon stem of i-tRNA, we made use of an earlier observation that overexpression of a 3GC mutant i-tRNA (having a wild type CAU anticodon) (Figure 7A) compromises *E. coli* growth and causes cold sensitivity (39). Here, we found that the growth of the strains sustained on either the IF3 (WT) or the IF3 mutant (R25A/Q33A/R66A) was affected by the 3GC mutant i-tRNA expression, but the toxicity was more severe in the mutant (Figure 7B) suggesting that the enhanced toxicity in the strains sustained on the mutant IF3 is due to its compromised activity in discriminating against the i-tRNA lacking 3GC base pairs and a higher level of non-productive binding of the 3GC mutant i-tRNA in the P-site. To confirm this, polysome fractions were analysed for the binding of the 3GC mutant i-tRNA to 70S ribosomal fractions. The amount of the 3GC mutant i-tRNA in the 30S was about the same in the strains sustained on either the wild type or the mutant IF3 (Figure 7C, compare lanes 1 and 4; and Supplementary Table S9). However, the amount of the 3GC mutant i-tRNA in the 70S fractions was about three folds higher in the strains sustained on the mutant (R25A/Q33A/R66A) IF3 than that on the wild type IF3 (Figure 7C, compare lanes 3 and 6; and Supplementary Table S9). These observations support that the mutant IF3 allows residency of the 3GC mutant i-tRNA during the transitions responsible for the conversion of the 30S pre-IC to the 70S complex.

IF3 NTD contributes to the eviction of IF3 CTD from the 30S subunit

The locations of IF3 binding on the 30S ribosome are dynamic, and IF3 undergoes conformational changes during 30S IC formation (12,40). An extended conformation represents the initial step in its binding to the 30S (without i-tRNA), wherein the CTD blocks the binding of 50S to the 30S. It has been shown that IF3 CTD alone is capable of anti-association activity, though it is not as efficient as the entire molecule (19). From the structural analyses, it is evident that the NTD does not have a direct role in the anti-association activity of IF3. However, it must regulate the movement of CTD on the ribosome through the linker. Interestingly, when we carried out polysome profiling, a diminished 70S peak with the concomitant increase in 30S and 50S peaks in the case of the IF3 mutant (R25A/Q33A/R66A) strain compared to the wild type IF3 also indicates a defect in subunit association (Figure 8A). To further investigate this, we checked the levels of IF3

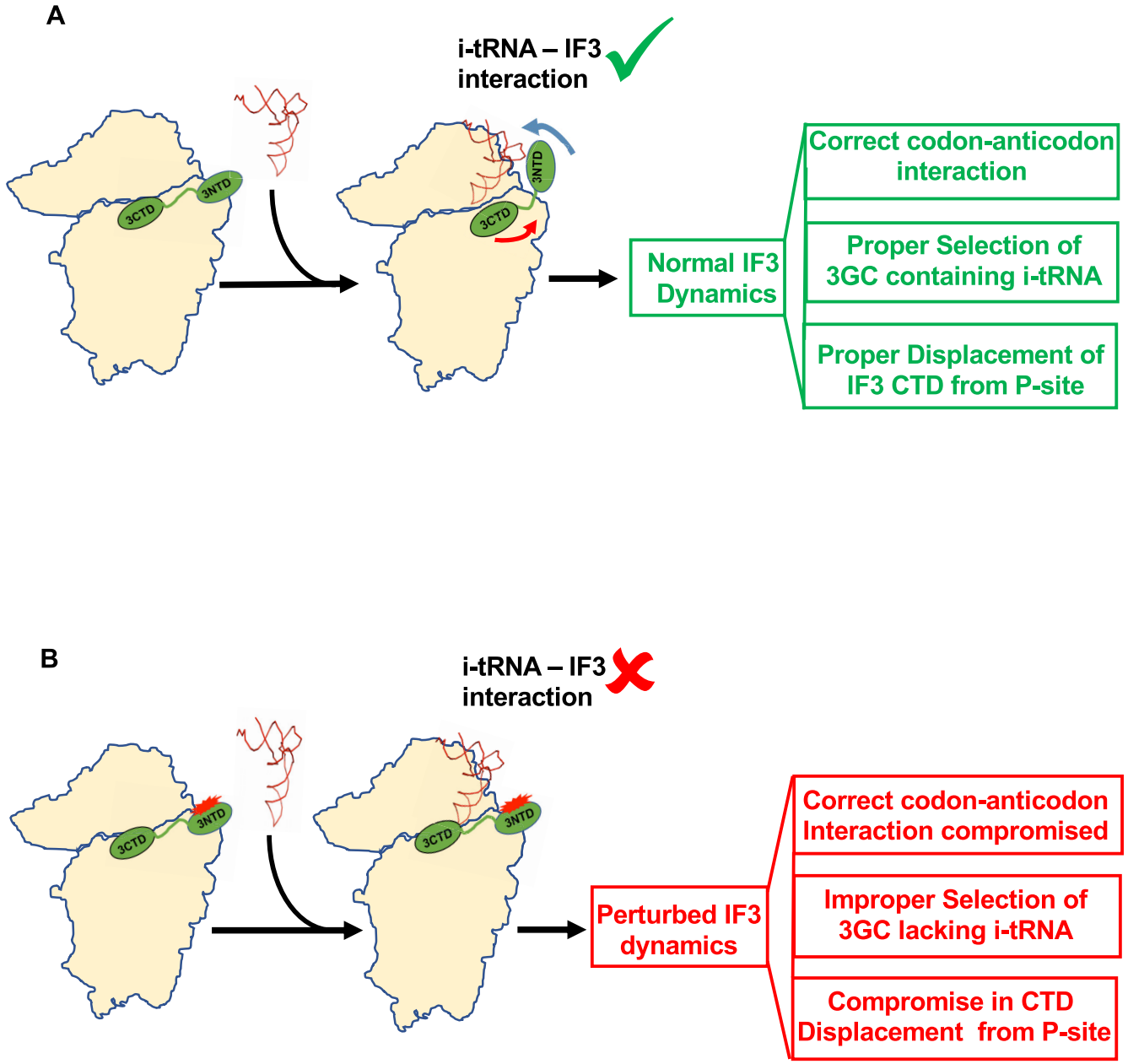

Figure 9. Model showcasing the importance of interaction between NTD and i-tRNA in translation initiation. (**A**) IF3 in an extended conformation on the 30S before binding of the i-tRNA. As the i-tRNA binds to 30S, the NTD relocate towards the elbow of the i-tRNA, but the CTD stays at the P-site. During the initiation pathway, the NTD moves along with the i-tRNA (depicted by a blue arrow) and coordinates the movement of CTD away from the P-site (shown by the red arrow). The normal IF3 dynamics observed in wild type is essential for the fidelity of initiation. (**B**) In the case of NTD mutant (red scar on NTD), the interaction between NTD and i-tRNA is disrupted. Hence, NTD is unlikely to move with i-tRNA during the initiation pathway perturbing its coordination with the CTD and the IF3 dynamics on the 30S. This alteration affects codon-anticodon selection, 3GC discrimination and the docking on 50S subunit.

bound to the polysome fractions. As opposed to the wild type, a significant amount of IF3 was found bound to the 30S fraction in the case of the mutant (Figure 8B), which may be the reason for the decreased subunit association. This high amount of IF3 (R25A/Q33A/R66A) mutant on 30S can occur in two possible ways, first due to increased binding affinity of the mutant towards free 30S ribosomal subunit, second because of decreased eviction rate of the mutant from 30S subunit. To test the first possibility, we performed in vitro binding of IF3 to 30S subunit in presence of other initiation factors. We found that there was no significant difference in the binding of wild type or the mutant IF3 towards 30S (Figures 8C and D) ruling out the first possibility. Thus, increased amount of IF3 mutant on 30S can be reasoned as a result of decreased eviction rate of the mutant from 30S caused by a slower IF3 dynamics in the absence of i-tRNA - NTD interaction. These observations suggest that coordination of NTD and CTD movements

through i-RNA is required for anti-association activity of IF3.

DISCUSSION

IF3 is an essential protein in bacteria. It is a *bona fide* anti-association factor, promotes 30S IC formation, prevents pseudo-initiation complex formation (20,41) and initiation from leaderless mRNAs (42). Further, IF3 is known to prevent initiation from non-canonical start codons and favour initiation from AUG, GUG, and UUG start codons (43,44). IF3 is also required for accurate i-tRNA selection at the P-site over elongator tRNAs (4). Notably, based on the biochemical studies, it was shown that all of these functions of IF3 could be carried by the CTD alone. And, the *in vivo* study also showed that the CTD alone is capable of sustaining *E. coli* for growth (24). On the other hand, the sequence of IF3 in its NTD are also well conserved. These observations present an evolutionary conundrum. The *in vivo* studies have also shown that the NTD plays an important role in the fidelity of initiation (21,24). More recently, it was also shown that the NTD plays a crucial role in recycling RbfA (45). However, the mechanism of how NTD facilitates IF3 functions in translation initiation remained unclear. The structural analyses of the 30S IC have shown that the NTD makes transient contacts with the elbow of i-tRNA during its accommodation in the P-site (12). The smFRET studies have also proposed that IF3 exists in three distinct conformational states on the 30S and a correctly base-paired i-tRNA at P-site permits an IF3 conformation, which allows efficient subunit joining due to unmasking of inter-subunit bride residues on 30S (40).

In this study, we carried out site-directed mutagenesis of the NTD to understand the mechanistic details of its role in different functions of IF3 by altering its interactions with i-tRNA elbow. The simulation runs show that these mutations do not change the structure of IF3 and have no impact on the interaction between the NTD and CTD of IF3 but can disrupt the interaction between NTD and i-tRNA (Figures 2 and 3); and the mutations compromise the cellular growth (Figure 4). Moreover, as seen from the increased initiation from non-canonical start codons such as AUU and AUA in the strains sustained on the IF3 mutants, the interactions of NTD with the i-tRNA play an important role in the start codon selection (Figure 5).

The binding of i-tRNA at the P-site is also determined by the presence of the 3GC base pairs in the anticodon stem of the i-tRNA (2). IF3 is known to play a role in discriminating against the tRNAs not having 3GC base pairs (18). Recently, we have also reported a mutation (V93A) is necessary in IF3 to allow initiation with a non-3GC i-tRNA (46). Although there is no direct interaction between IF3 and 3GC base pairs, this discrimination is most likely modulated through the interaction of 3GC base pairs with G1338 and A1339 of the 16S rRNA during i-tRNA accommodation (17). In our CAT reporter assays, the mutations in NTD lead to increased initiation by the 3GC mutant i-tRNA (Figure 6). Likewise, a compromised NTD activity allowed the 3GC mutant i-tRNA to be retained during the 30S to 70S transitions (Figure 7C). These observations support a regulatory role for NTD in the scrutiny of the 3GC base pairs in i-tRNA.

The individual domains of IF3 show well-ordered dynamics on the 30S subunit, which ensures precise translation of mRNA (33). Our observations show how the two domains of IF3 work in conjunction to allow initiation, a process that is compromised if the interactions of the NTD with the i-tRNA are disrupted (Figures 5 and 6). The disruption of the interactions also compromised the dislodgement of the CTD from the P-site (Figure 8). The formation of 70S IC, a rate limiting step, is regulated by displacing the CTD from the P-site (33). A flawed CTD displacement from the P-site might also decrease the rate of 70S IC formation. Our study highlights the importance of the interactions between the elbow of i-tRNA and NTD in the coordinating the movements of NTD and CTD through i-tRNA and thus modulating CTD displacement during translation initiation (Figure 9). Based on the cryo-EM studies, it is known that i-tRNA and IF3 undergo large-scale movement during the accommodation of i-tRNA in the P-site (12). We propose that the interactions between the i-tRNA and the NTD of IF3 are crucial for the large-scale movement of the CTD during the process of i-tRNA accommodation and therefore for the function of IF3 during the process of initiation. A disruption in the interactions of i-tRNA with the NTD would fail to synchronize the movement of the i-tRNA with the CTD resulting in the compromised function of IF3. In such a model, the linker between the NTD and CTD would be expected to play an important role in the overall function of IF3. Interestingly, earlier studies have shown that the linker region is indeed important for the proper functioning of IF3 (47). In conclusion, our observations suggest that interaction between NTD and i-tRNA ensures coordination of NTD and CTD movements and this interaction is critical for various functions of IF3 in initiation.

DATA AVAILABILITY

The data underlying this article will be shared on reasonable request to the corresponding author.

SUPPLEMENTARY DATA

Supplementary Data are available at NAR Online.

ACKNOWLEDGEMENTS

The authors acknowledge laboratory colleagues for their critical comments on the manuscript. The funders had no role in study design, data collection and analysis, or decision to its publication.

FUNDING

Science and Engineering Research Board [EMR/2016/005617]; Department of Biotechnology [BT/PR28058, BT/PR13522]; Jamsetji Tata Trust [R(HR)Tata Chairs/2020–854/78]; U.V. is a J.N. Tata Chair Professor and a J.C. Bose Fellow; T.H. is supported by Wellcome Trust/DBT India Alliance Fellowship (IA/I/17/2/503313);

DBT-IISc Partnership Program Phase-II [BT/PR27952-INF/22/212/2018]; DST-FIST level II infrastructure support. Funding for open access charge: Research Grants.
Conflicts of interest statement. None declared.

REFERENCES

1. RajBhandary,U.L. (1994) Initiator transfer RNAs. *J. Bacteriol.***176**, 547–552.
2. Mandal,N., Mangroo,D., Dalluge,J.J., McCloskey,J.A. and RajBhandary,U.L. (1996) Role of the three consecutive G:C base pairs conserved in the anticodon stem of initiator tRNAs in initiation of protein synthesis in *Escherichia coli*. *RNA*, **2**, 473–482.
3. Carter,A.P., Clemons,J., Brodersen,D.E., Morgan-Warren,R.J., Hartsch,T., Wimberly,B.T. and Ramakrishnan,V. (2001) Crystal structure of an initiation factor bound to the 30S ribosomal subunit. *Science*, **291**, 498–501.
4. Antoun,A., Pavlov,M.Y., Lovmar,M. and Ehrenberg,M. (2006) How initiation factors tune the rate of initiation of protein synthesis in bacteria. *EMBO J.*, **25**, 2539–2550.
5. Milon,P., Carotti,M., Konevega,A.L., Wintermeyer,W., Rodnina,M.V. and Gualerzi,C.O. (2010) The ribosome-bound initiation factor 2 recruits initiator tRNA to the 30S initiation complex. *EMBO Rep.*, **11**, 312–316.
6. Sprink,T., Ramrath,D.J.F., Yamamoto,H., Yamamoto,K., Loerke,J., Ismer,J., Hildebrand,P.W., Scheerer,P., Bürger,J., Mielke,T. *et al.* (2016) Structures of ribosome-bound initiation factor 2 reveal the mechanism of subunit association. *Sci. Adv.*, **2**, e150150.
7. Laursen,B.S., Sørensen,H.P., Mortensen,K.K. and Sperling-Petersen,H.U. (2005) Initiation of protein synthesis in bacteria. *Microbiol. Mol. Biol. Rev.*, **69**, 101–123.
8. Selmer,M., Dunham,C.M., Murphy IV,F.V., Weixlbaumer,A., Petry,S., Kelley,A.C., Weir,J.R. and Ramakrishnan,V. (2006) Structure of the 70S ribosome complexed with mRNA and tRNA. *Science*, **313**, 1935–1942.
9. Gualerzi,C.O. and Pon,C.L. (2015) Initiation of mRNA translation in bacteria: structural and dynamic aspects. *Cell. Mol. Life Sci.*, **72**, 4341–4367.
10. Subramanian,A.R. and Davis,B.D. (1970) Activity of initiation factor F3 in dissociating *Escherichia coli* ribosomes. *Nature*, **228**, 1273–1275.
11. Liu,Q. and Fredrick,K. (2015) Roles of helix H69 of 23S rRNA in translation initiation. *Proc. Natl. Acad. Sci. U.S.A.*, **112**, 11559–11564.
12. Hussain,T., Llácer,J.L., Wimberly,B.T., Kieft,J.S. and Ramakrishnan,V. (2016) Large-Scale movements of IF3 and tRNA during bacterial translation initiation. *Cell*, **167**, 133–144.
13. Moreau,M., De Cock,E., Fortier,P.L., Garcia,C., Albaret,C., Blanquet,S., Lallemand,J.Y. and Dardel,F. (1997) Heteronuclear NMR studies of *E. coli* translation initiation factor IF3. Evidence that the inter-domain region is disordered in solution. *J. Mol. Biol.*, **266**, 15–22.
14. Fortier,P.L., Schmitter,J.M., Garcia,C. and Dardel,F. (1994) The N-terminal half of initiation factor IF3 is folded as a stable independent domain. *Biochimie*, **76**, 376–383.
15. Julián,P., Milon,P., Agirrezabala,X., Lasso,G., Gil,D., Rodnina,M.V. and Valle,M. (2011) The cryo-EM structure of a complete 30S translation initiation complex from *Escherichia coli*. *PLoS Biol.*, **9**, e1001095.
16. Mccutcheon,J.P., Agrawal,R.K., Philips,S.M., Grassucci,R.A., Gerchman,S.E., Clemons,W.M., Ramakrishnan,V. and Frank,J. (1999) Location of translational initiation factor IF3 on the small ribosomal subunit. *Proc. Natl. Acad. Sci. U.S.A.*, **96**, 4301–4306.
17. Lancaster,L. and Noller,H.F. (2005) Involvement of 16S rRNA nucleotides G1338 and A1339 in discrimination of initiator tRNA. *Mol. Cell*, **20**, 623–632.
18. O'Connor,M., Gregory,S.T., Rajbhandary,U.L. and Dahlberg,A.E. (2001) Altered discrimination of start codons and initiator tRNAs by mutant initiation factor 3. *RNA*, **7**, 969–978.
19. Petrelli,D., La Teana,A., Garofalo,C., Spurio,R., Pon,C.L. and Gualerzi,C.O. (2001) Translation initiation factor IF3: two domains, five functions, one mechanism? *EMBO J.*, **20**, 4560–4569.
20. Hartz,D., McPheeters,D.S. and Gold,L. (1989) Selection of the initiator tRNA by *Escherichia coli* initiation factors. *Genes Dev.*, **3**, 1899–1912.
21. Maar,D., Liveris,D., Sussman,J.K., Ringquist,S., Moll,I., Heredia,N., Kil,A., Bläsi,U., Schwartz,I. and Simons,R.W. (2008) A single mutation in the IF3 N-Terminal domain perturbs the fidelity of translation initiation at three levels. *J. Mol. Biol.*, **383**, 937–944.
22. Sacerdot,C., De Cock,E., Engst,K., Graffe,M., Dardel,F. and Springer,M. (1999) Mutations that alter initiation codon discrimination by *Escherichia coli* initiation factor IF3. *J. Mol. Biol.*, **288**, 803–810.
23. De Bellis,D., Liveris,D., Schwartz,I., Goss,D. and Ringquist,S. (1992) Structure-Function analysis of *Escherichia coli* translation initiation factor IF3: tyrosine 107 and lysine 110 are required for ribosome binding. *Biochemistry*, **31**, 11984–11990.
24. Ayyub,S.A., Dobriyal,D. and Varshney,U. (2017) Contributions of the N-and C-terminal domains of initiation factor 3 to its functions in the fidelity of initiation and antiassociation of the ribosomal subunits. *J. Bacteriol.*, **199**, e00051-17.
25. Kaledhonkar,S., Fu,Z., Caban,K., Li,W., Chen,B., Sun,M., Gonzalez,R.L. and Frank,J. (2019) Late steps in bacterial translation initiation visualized using time-resolved cryo-EM. *Nat.*, **570**, 400–404.
26. Maier,J.A., Martinez,C., Kasavajhala,K., Wickstrom,L., Hauser,K.E. and Simmerling,C. (2015) ff14SB: improving the accuracy of protein side chain and backbone parameters from ff99SB. *J. Chem. Theory Comput.*, **11**, 3696–3713.
27. Zgarbová,M., Otyepka,M., Šponer,J., Mládek,A., Banáš,P., Cheatham,T.E. and Jurečka,P. (2011) Refinement of the cornell et al. Nucleic acids force field based on reference quantum chemical calculations of glycosidic torsion profiles. *J. Chem. Theory Comput.*, **7**, 2886–2902.
28. Bonomi,M., Bussi,G., Camilloni,C., Tribello,G.A., Banáš,P., Barducci,A., Bernetti,M., Bolhuis,P.G., Bottaro,S., Branduardi,D. *et al.* (2019) Promoting transparency and reproducibility in enhanced molecular simulations. *Nat. Methods*, **16**, 670–673.
29. Datsenko,K.A. and Wanner,B.L. (2000) One-step inactivation of chromosomal genes in *Escherichia coli* K-12 using PCR products. *Proc. Natl. Acad. Sci. U.S.A.*, **97**, 6640–6645.
30. Das,G., Thotala,D.K., Kapoor,S., Karunanithi,S., Thakur,S.S., Singh,N.S. and Varshney,U. (2008) Role of 16S ribosomal RNA methylations in translation initiation in *Escherichia coli*. *EMBO J.*, **27**, 840–851.
31. Macdougall,D.D. and Gonzalez,R.L. (2015) Translation initiation factor 3 regulates switching between different modes of ribosomal subunit joining. *J. Mol. Biol.*, **427**, 1801–1818.
32. Milon,P., Konevega,A.L., Peske,F., Fabbretti,A., Gualerzi,C.O. and Rodnina,M.V. (2007) Transient kinetics, fluorescence, and FRET in studies of initiation of translation in bacteria. *Methods Enzymol.*, **430**, 1–30.
33. Nakamoto,J.A., Evangelista,W., Vinogradova,D.S., Konevega,A.L., Spurio,R., Fabbretti,A. and Milón,P. (2021) The dynamic cycle of bacterial translation initiation factor IF3. *Nucleic Acids Res.*, **49**, 6958–6970.
34. Lesage,P., Truong,H.N., Graffe,M., Dondon,J. and Springer,M. (1990) Translated translational operator in *Escherichia coli* auto-regulation in the infC-rpmI-rplT operon. *J. Mol. Biol.*, **213**, 465–475.
35. Hecht,A., Glasgow,J., Jaschke,P.R., Bawazer,L.A., Munson,M.S., Cochran,J.R., Endy,D. and Salit,M. (2017) Measurements of translation initiation from all 64 codons in *E. coli*. *Nucleic Acids Res.*, **45**, 3615–3626.
36. Meinnel,T., Sacerdot,C., Graffe,M., Blanquet,S. and Springer,M. (1999) Discrimination by *Escherichia coli* initiation factor IF3 against initiation on non-canonical codons relies on complementarity rules. *J. Mol. Biol.*, **290**, 825–837.
37. Datta,M., Pillai,M., Modak,M.J., Liiv,A., Khaja,F.T., Hussain,T., Remme,J. and Varshney,U. (2021) A mutation in the ribosomal protein uS12 reveals novel functions of its universally conserved PNSA loop. *Mol. Microbiol.*, **115**, 1292–1308.
38. Varshney,U. and RajBhandary,U.L. (1990) Initiation of protein synthesis from a termination codon. *Proc. Natl. Acad. Sci. U.S.A.*, **87**, 1586–1590.

39. Shetty,S. and Varshney,U. (2016) An evolutionarily conserved element in initiator trnas prompts ultimate steps in ribosome maturation. *Proc. Natl. Acad. Sci. U.S.A.*, **113**, E6126–E6134.
40. Elvekrog,M.M. and Gonzalez,R.L. (2013) Conformational selection of translation initiation factor 3 signals proper substrate selection. *Nat. Struct. Mol. Biol.*, **20**, 628–633.
41. Gualerzi,C., Risuleo,G. and Pon,C.L. (1977) Initial rate kinetic analysis of the mechanism of initiation complex formation and the role of initiation factor IF-3. *Biochemistry*, **16**, 1684–1689.
42. Tedin,K., Moll,I., Grill,S., Resch,A., Graschopf,A., Gualerzi,C.O. and Bläsi,U. (1999) Translation initiation factor 3 antagonizes authentic start codon selection on leaderless mRNAs. *Mol. Microbiol.*, **31**, 67–77.
43. Teana,A.La, Pon,C.L. and Gualerzi,C.O. (1993) Translation of mRNAs with degenerate initiation triplet AUU displays high initiation factor 2 dependence and is subject to initiation factor 3 repression. *Proc. Natl. Acad. Sci. U.S.A.*, **90**, 4161–4165.
44. Grigoriadou,C., Marzi,S., Pan,D., Gualerzi,C.O. and Cooperman,B.S. (2007) The translational fidelity function of IF3 during transition from the 30 s initiation complex to the 70 s initiation complex. *J. Mol. Biol.*, **373**, 551–561.
45. Sharma,I.M. and Woodson,S.A. (2020) RbfA and IF3 couple ribosome biogenesis and translation initiation to increase stress tolerance. *Nucleic Acids Res.*, **48**, 359–372.
46. Datta,M., Singh,J., Modak,M.J., Pillai,M. and Varshney,U. (2022) Systematic evolution of initiation factor 3 and the ribosomal protein uS12 optimizes *Escherichia coli* growth with an unconventional initiator tRNA. *Mol. Microbiol.*, **117**, 462–479.
47. De Cock,E., Springer,M. and Dardel,F. (1999) The interdomain linker of *Escherichia coli* initiation factor IF3: a possible trigger of translation initiation specificity. *Mol. Microbiol.*, **32**, 193–202.